


Measurement of $\sigma(e^+e^- \rightarrow HZ) \times \mathcal{B}r(H \rightarrow ZZ^*)$ at the 250 GeV ILC

E. Antonov[✉] and A. Drutskoy[✉]

P.N. Lebedev Physical Institute of the Russian Academy of Sciences, Moscow 119991, Russia

 (Received 23 August 2021; accepted 15 October 2021; published 18 November 2021)

We report on studies of the $e^+e^- \rightarrow HZ$ process with the subsequent decay of the Higgs boson $H \rightarrow ZZ^*$, where the ZZ^* combination is reconstructed in the final states with two jets and two leptons. The analysis is performed using Monte Carlo data samples obtained with detailed ILD detector simulation assuming the integrated luminosity 2 ab^{-1} , the beam polarizations $\mathcal{P}_{e^-e^+} = (-0.8, +0.3)$, and the center-of-mass energy $\sqrt{s} = 250 \text{ GeV}$. The analysis is also repeated for the case of two 0.9 ab^{-1} data samples with polarizations $\mathcal{P}_{e^-e^+} = (\mp 0.8, \pm 0.3)$. The process is measured in four decay channels, which correspond to two combinations for the Higgs final states and two decay modes of the directly produced Z boson, $Z \rightarrow q\bar{q}$ and $Z \rightarrow \nu\bar{\nu}$. To obtain the Higgs boson mass distributions, we used the variables $M(jj\ell\ell)$ and $M_\Delta = M(jj\ell\ell) - M(jj) + M(Z_{\text{nom}})$, where $M(Z_{\text{nom}}) = 91.2 \text{ GeV}$. Contributions of the potential background processes are taken into account based on the available MC event samples. We propose a model-independent method for obtaining the width of the Higgs boson using the measurement of the $e^+e^- \rightarrow HZ$ process.

DOI: [10.1103/PhysRevD.104.093007](https://doi.org/10.1103/PhysRevD.104.093007)

I. INTRODUCTION

Since the discovery of the Higgs boson by the ATLAS and CMS collaborations [1,2] in 2012, the next important task is to measure parameters of this particle with the highest possible accuracy. In recent years, the mass, couplings, production cross sections, and quantum numbers of the Higgs boson have been measured in the LHC experiments with increasing accuracies. However, the width of the Higgs boson is difficult to measure at LHC in a model-independent approach. Indirect methods will be used to measure the Higgs width at LHC after the high-luminosity upgrade, but even with the data sample of 3 ab^{-1} the uncertainty is expected to be $\sim 20\%$ [3,4].

The width of the Higgs boson is strictly theoretically defined within the Standard Model (SM) for a fixed Higgs mass. The width value of $4.1 \text{ MeV}/c^2$ has been calculated for the mass of $125 \text{ GeV}/c^2$ [5]. This result may be distorted by beyond the Standard Model (BSM) contributions. Therefore, the model-independent measurement of the Higgs width provides an important test of SM. A high accuracy of the Higgs width measurement can be reached at the future e^+e^- linear collider ILC [6,7]. A large number of Higgs bosons will be produced at ILC, whereas backgrounds are expected to be relatively small. Events in the

ILD detector [8] at ILC have clean and well-defined signatures and, therefore, processes of interest can be identified and studied in detail.

We propose to use the process $e^+e^- \rightarrow ZH$ with the subsequent decay $H \rightarrow ZZ^*$ to measure the product of the cross section and the decay branching fraction, which can theoretically be expressed as:

$$\sigma(e^+e^- \rightarrow HZ) \times \mathcal{B}r(H \rightarrow ZZ^*) = C \cdot g_Z^4 / \Gamma_H. \quad (1)$$

Here C is a constant which can be calculated theoretically with an uncertainty of less than 1% [7], g_Z is the Higgs boson coupling HZZ , and Γ_H is the Higgs boson width. Therefore, the measurement of this product can be used to obtain the width of the Higgs boson with a high accuracy, because the coupling g_Z is expected to be determined combining ILC and LHC results with an uncertainty of about 0.5% [9] using other processes. In this analysis we assume the data sample of 2 ab^{-1} collected by the ILD experiment in the e^+e^- collisions at a center-of-mass energy 250 GeV. The accuracy of the $e^+e^- \rightarrow ZH$ process measurement at 250 GeV with the subsequent decay $H \rightarrow ZZ^*$ has also been evaluated using the SiD detector simulation [6].

In the studied process the two on-shell Z bosons and one off-shell Z^* boson have to be reconstructed. The directly produced Z boson is denoted below as Z_1 to separate it from the Z bosons produced in the Higgs decay. The decays of the $Z_{(1)}^{(*)}$ bosons to two hadronic jets, two opposite sign leptons ($\ell^\pm = e^\pm, \mu^\pm$), and two neutrinos are considered in

Published by the American Physical Society under the terms of the Creative Commons Attribution 4.0 International license. Further distribution of this work must maintain attribution to the author(s) and the published article's title, journal citation, and DOI. Funded by SCOAP³.

the analysis. The number of signal events is expected to be small if two of these three $Z_{(1)}^{(*)}$ bosons are reconstructed in leptonic modes. Therefore we reconstruct only one of three $Z_{(1)}^{(*)}$ bosons in the leptonic mode, and other two in hadronic or neutrino modes. In this paper four channels are studied and the final precision of the Higgs width measurement is calculated combining accuracies obtained in these channels.

II. MC SAMPLES AND ANALYSIS TOOLS

In this analysis we study the following subprocesses:

$$e^+e^- \rightarrow Z_1(q_1q_2)H, \quad H \rightarrow Z(q_3q_4)Z^*(\ell_1\ell_2) \quad (2)$$

$$e^+e^- \rightarrow Z_1(q_1q_2)H, \quad H \rightarrow Z(\ell_1\ell_2)Z^*(q_3q_4) \quad (3)$$

$$e^+e^- \rightarrow Z_1(\nu\bar{\nu})H, \quad H \rightarrow Z(q_1q_2)Z^*(\ell_1\ell_2) \quad (4)$$

$$e^+e^- \rightarrow Z_1(\nu\bar{\nu})H, \quad H \rightarrow Z(\ell_1\ell_2)Z^*(q_1q_2) \quad (5)$$

The official Monte Carlo (MC) data samples produced by the ILD group are used. All processes are generated using WHIZARD 2.8.5 package [10] with the LCIO [11] output format; hadronization is performed by PYTHIA 6 [12]. The detailed simulation of the ILD detector effects is performed using the ILD_15_01_v02 model from the ILCSOft toolkit [13] v02-00-02 using the DD4HEP [14]

software package. Finally, the events are reconstructed with the MarlinReco [15] package.

The official MC samples are generated assuming four possible combinations with 100% beam polarization, $\mathcal{P}_{e^-e^+} = (\pm 1.0, \pm 1.0)$, and 250 GeV center-of-mass energy. For the signal events two sets of MC samples are obtained: $e_L^-e_R^+$ (LR) with left-handed electrons and right-handed positrons and $e_R^-e_L^+$ (RL) with right-handed electrons and left-handed positrons. Initial state radiation (ISR) and beam radiation processes are properly included at the generation level. The $\gamma\gamma$ beam induced processes are overlaid on the generated events before reconstruction. The MC samples contain data arrays, so-called data collections, with information about all particles in an event. In particular, the MCParticles [16] and PandoraPFOs (the Particle Flow Objects reconstructed with PandoraPFA [17]) collections are included in the samples. Table I shows the basic information taken from logbook ELOG [18] for MC samples selected from repository for this analysis. Zero background contribution is obtained in studies of the MC samples $ZZ(4j) + \gamma^*(2\ell)$, $ZZ/WW(4j) + 2\nu$, $H(all) + X$, and $Z(2\nu)Z(2j) + \gamma^*(2\ell)$, which are not included in Table I.

ILCSOft includes the Marlin software package, which contains special program codes, so-called processors, used, in particular, for the separation of isolated leptons and the jet reconstruction. The Marlin package provides an option to use the FastJet [19] software codes, designed for clustering particles in jets based on various reconstruction algorithms. This method is used in the analysis.

TABLE I. The basic information for all MC samples used in the analysis. The numbers are taken from generation logbook ELOG. The given cross sections are corrected for the decay branching fractions indicated in the first column. The upper and down quarks are labeled as q_u and q_d respectively.

Process	Integrated luminosity, ab^{-1}				Cross section, fb				Number of events			
	eLpR	eRpL	eLpL	eRpR	eLpR	eRpL	eLpL	eRpR	eLpR	eRpL	eLpL	eRpR
	Signal samples											
$q\bar{q}H(ZZ)$	55.6	86.9			8.99	5.75			$5 \cdot 10^5$	$5 \cdot 10^5$		
$\nu_e\bar{\nu}_eH(ZZ)$	316	889			1.58	0.56			$5 \cdot 10^5$	$5 \cdot 10^5$		
$\nu_{\mu\tau}\bar{\nu}_{\mu\tau}H(ZZ)$	284	445			1.76	1.12			$5 \cdot 10^5$	$5 \cdot 10^5$		
	Background samples											
$q\bar{q}$	5.00	5.00			$128 \cdot 10^3$	$70.4 \cdot 10^3$			$6.40 \cdot 10^8$	$3.52 \cdot 10^8$		
$W(q\bar{q})W(e + \nu)$	5.00	5.77	1.05	1.05	$10.3 \cdot 10^3$	86.7	191	191	$51.4 \cdot 10^6$	$5 \cdot 10^5$	$2 \cdot 10^5$	$2 \cdot 10^5$
$W(q\bar{q})W(\mu/\tau + \nu)$	5.00	5.19			$18.8 \cdot 10^3$	173			$93.9 \cdot 10^6$	$9 \cdot 10^5$		
$Z(q\bar{q})Z(e^+e^-)$	5.06	5.00	1.04	1.04	1423	1219	1156	1157	$72 \cdot 10^5$	$61 \cdot 10^5$	$12 \cdot 10^5$	$12 \cdot 10^5$
$Z(q\bar{q})Z(\mu^+\mu^-/\tau^+\tau^-)$	5.01	5.14			838	467			$42 \cdot 10^5$	$24 \cdot 10^5$		
$WW/ZZ(q_u\bar{q}_d\bar{q}_uq_d)$	5.00	5.32			$12.4 \cdot 10^3$	225			$62 \cdot 10^6$	$12 \cdot 10^5$		
WW (other 4q)	5.00	5.12			$14.8 \cdot 10^3$	225			$74.4 \cdot 10^6$	$7 \cdot 10^5$		
ZZ (other 4q)	5.05	5.11			1406	607			$7.1 \cdot 10^6$	$3.1 \cdot 10^6$		
$WW(4q) + \gamma^*(e^+e^-)$	28.1	168	183	182	0.71	0.12	0.11	0.11	$2 \cdot 10^4$	$2 \cdot 10^4$	$2 \cdot 10^4$	$2 \cdot 10^4$
$WW(4q) + \gamma^*(\mu^+\mu^-/\tau^+\tau^-)$	16.9	407			1.19	0.05			$2 \cdot 10^4$	$2 \cdot 10^4$		
$q\bar{q}H$ (all)	1.5	2.3			343	219			$5 \cdot 10^5$	$5 \cdot 10^5$		

III. EVENT PRESELECTION AND INITIAL ANALYSIS

The MC samples studied are preselected using the MCParticle collection containing information from the MC event generator level. The signal samples are extracted requiring only specific process and decay chains. The background samples are studied without preselections, however the most dangerous background processes are also preselected and studied separately. All following selections are applied using the information on the reconstruction level.

The first step of the event selection is to identify two isolated lepton candidates. The standard `IsolatedLeptonTagging` [20] processor is applied for this goal. This processor finds high energy leptons in events using multivariate double-cone method and TMVA [21] machine learning algorithms. We used the default set of parameters and weights included in this processor. The Z^* and Z reconstruction efficiencies in the leptonic modes in the channel with four jets (two jets) are $\sim 67\%$ ($\sim 72\%$) and $\sim 90\%$ ($\sim 91\%$), respectively. Only events with two identified isolated leptons are kept for the following analysis. These leptons are excluded from the following jet reconstruction procedure.

Energetic ISR photons can be observed inside the detector, this can affect the analysis. A simple ISR identification procedure [22] is applied after the lepton identification procedure. If an ISR photon candidate is found, it is removed from the PFOs collection and not used in the jet reconstruction.

The next step is the jet reconstruction which is performed using `FastJet` clustering tools. For this goal we choose the Valencia [23] algorithm, which was specially developed for jet reconstruction at electron-positron colliders. We select this algorithm for its high efficiency of jet reconstruction near the beam direction. After excluding isolated leptons and ISR photons all remaining particles in an event are expected to be a part of jets or to come from a $\gamma\gamma$ low P_t process. On average about $0.4\gamma\gamma$ low P_t hadron events are expected per bunch-crossing at $\sqrt{s} = 250$ GeV [24]. We use an exclusive k_T clustering algorithm [25] with a generalized jet radius of 1.5 to remove the $\gamma\gamma$ overlay particles and the Valencia algorithm to force the remaining particles into two or four jets, depending on the studied channel. Three parameters should be adjusted in the Valencia algorithm, the generalized jet cone radius R , and the β and γ parameters, which are used to control the clustering order and the background resilience. We set the β parameter to 1.0 that corresponds to behavior of the k_T algorithm. The radius R and the parameter γ are tuned to optimize the invariant two-jet mass shape from the $Z \rightarrow jj$ decay. The position and the width of the two-jet mass distribution are evaluated for different R and γ values using the $M(jj) - M(Z)$, IQR_{34} , RMS_{90} and Median parameters proposed in [23]. We chose the values of these parameters which provide the best Z boson mass reconstruction

TABLE II. The best Valencia algorithm parameters chosen for the jet reconstruction in different channels.

Valencia parameters	$Z_1(jj)$, $Z(jj)$, $Z^*(\ell\ell)$	$Z_1(jj)$, $Z(\ell\ell)$, $Z^*(jj)$	$Z_1(\nu\bar{\nu})$, $Z(jj)$, $Z^*(\ell\ell)$	$Z_1(\nu\bar{\nu})$, $Z(\ell\ell)$, $Z^*(jj)$
β	1.0	1.0	1.0	1.0
γ	0.4	0.4	0.6	0.3
R	1.6	0.7	1.4	1.4

quality. Table II shows the sets of the best R , β and γ parameters chosen for the Valencia jet clustering algorithm in each channel.

The product of the cross section and the branching fraction discussed above can be measured experimentally using the formula:

$$\sigma(e^+e^- \rightarrow HZ_1) \times Br(H \rightarrow ZZ^*) = N_{\text{sig}} / (\mathcal{L}_{\text{int}} \cdot \epsilon \cdot Br(Z_1) \cdot Br(Z) \cdot Br(Z^*)) \quad (6)$$

where N_{sig} is the number of signal events measured in a specific channel, and \mathcal{L}_{int} is the integrated luminosity of a used data sample. For a studied channel the selection efficiency is denoted by ϵ and the relevant decay branching fractions of the Z bosons decays taken from PDG [3] are denoted as $Br(Z_1)$, $Br(Z)$, and $Br(Z^*)$.

To get the expected number of signal or background events with $P_{e^-e^+} = (-0.8, +0.3)$ polarization and the integrated luminosity 2 ab^{-1} , we apply a weight factor to each event from the MC samples. The MC samples are generated assuming 100% polarized beams; the sample nominal integrated luminosities \mathcal{L}_{nom} are given in Table I. The weight factor W is calculated as:

$$W = \left[\frac{1 \pm 0.8}{2} \cdot \frac{1 \pm 0.3}{2} \right] \cdot \frac{2 \text{ ab}^{-1}}{\mathcal{L}_{\text{nom}}} \quad (7)$$

The numbers of initial MC events, the numbers of events remained after lepton identification, the weight factors, and the final number of weighted events are given in Table III.

The number of Higgs boson signal events is obtained by fitting distributions of the invariant mass $M(jj\ell\ell)$. However for the channels with $Z \rightarrow jj$ and $Z^* \rightarrow \ell\ell$ decays the following formula gives a better resolution:

$$M_{\Delta} = M(jj\ell\ell) - M(jj) + M(Z_{\text{nom}}) \quad (8)$$

where $M(Z_{\text{nom}}) = 91.2$ GeV. This formula results in a narrower Higgs boson mass peak, because uncertainties of the jet reconstruction are mostly canceled in the mass difference.

TABLE III. The numbers of signal events before cuts for different final states obtained from MC samples with different polarizations before and after lepton tagging and reweighting. The integrated luminosity 2 ab^{-1} and polarization $\mathcal{P}_{e^-e^+} = (-0.8, +0.3)$ is assumed.

Channels	$\mathcal{P}_{e^-e^+}$	MC events	Lepton tagging, events	Weight factors	Weighted number of events
$Z_1(jj),$ $Z(jj),$ $Z^*(\ell\ell)$	eLpR eRpL	23989 23845	16088 16027	2.1×10^{-2} 1.3×10^{-3}	338 21
$Z_1(jj),$ $Z(\ell\ell),$ $Z^*(jj)$	eLpR eRpL	23261 23132	20879 20664	2.1×10^{-2} 1.3×10^{-3}	439 27
$Z_1(\nu_e\bar{\nu}_e),$ $Z(jj),$ $Z^*(\ell\ell)$	eLpR eRpL	24044 23910	17429 17259	3.7×10^{-3} 7.9×10^{-5}	65 1.4
$Z_1(\nu_e\bar{\nu}_e),$ $Z(\ell\ell),$ $Z^*(jj)$	eLpR eRpL	23059 23096	21108 21149	3.7×10^{-3} 7.9×10^{-5}	79 1.7
$Z_1(\nu_{\mu,\tau}\bar{\nu}_{\mu,\tau}),$ $Z(jj),$ $Z^*(\ell\ell)$	eLpR eRpL	23840 23862	17103 17168	4.1×10^{-3} 1.6×10^{-4}	71 2.7
$Z_1(\nu_{\mu,\tau}\bar{\nu}_{\mu,\tau}),$ $Z(\ell\ell),$ $Z^*(jj)$	eLpR eRpL	23189 23225	21168 21246	4.1×10^{-3} 1.6×10^{-4}	88 3.3

IV. RESULTS

The four channels are studied and the signal statistical uncertainties are evaluated. To suppress backgrounds various cuts are applied as summarized in Table IV. First, the signal and background distributions are obtained with the weighted bin contents and uncertainties. These distributions are fitted to obtain shape parameters separately for the signal and background. Then, the signal statistical uncertainties are estimated using the obtained distribution shapes and normalizations. To reproduce the real data distribution, the weighted signal and background distributions are summed, the content of each bin is rounded to the integer number and the Poisson uncertainties for the bin contents are assumed. The binned extended maximum likelihood fit method is applied to the combined distributions with the function including signal and background terms with the fixed shapes determined in the first step and free normalizations. Finally, the toy MC method is applied to obtain precise estimates for the signal statistical uncertainties.

A. Study of the $e^+e^- \rightarrow Z_1(j_1j_2)H(ZZ^*)$ process with $Z \rightarrow j_3j_4, Z^* \rightarrow \ell^+\ell^-$

The final state of the first studied channel includes two leptons and four jets. To form the Z_1 and Z bosons from

TABLE IV. The sets of selections used for each studied channel are shown.

Selection	$Z_1(jj),$ $Z(jj),$ $Z^*(\ell\ell)$	$Z_1(jj),$ $Z(\ell\ell),$ $Z^*(jj)$	$Z_1(\nu\bar{\nu}),$ $Z(jj),$ $Z^*(\ell\ell)$	$Z_1(\nu\bar{\nu}),$ $Z(\ell\ell),$ $Z^*(jj)$
$M(\ell\ell)$ (GeV/c ²)	[13, 36]	[70, 95]	[13, 34]	[80, 95]
$M(Z \rightarrow jj)$ (GeV/c ²)	> 70	< 50	[80, 113]	[13, 38]
$M(Z_1 \rightarrow jj)$ (GeV/c ²)	> 70	> 70		
$E(jjjj\ell\ell)$ (GeV)	[200, 260]	[200, 260]		
$E(jj\ell\ell)$ (GeV)			< 145	< 145
$P_{\max}(\ell)$ (GeV/c)	< 32		< 40	
$P_{\min}(\ell)$ (GeV/c)	> 9		> 8	
$P_{\max}(j_1)$ (GeV/c)				< 22
$P_{\max}(j_2)$ (GeV/c)				< 42
$P(jj\ell\ell)$ (GeV/c)			[30, 70]	[40, 70]
$ \cos \theta_{\text{vis}} $			< 0.8	< 0.9
$\Delta\phi_{ZZ^*}$ (degree)			< 120	< 140

these four jets we calculate χ^2 for six possible two-jet combinations:

$$\chi^2 = \frac{(M(Z_1) - M(Z_{\text{nom}}))^2}{\sigma^2 M_{Z_1}} + \frac{(M(Z) - M(Z_{\text{nom}}))^2}{\sigma^2 M_Z} + \frac{(P(Z_1) - \bar{P}(Z_1))^2}{\sigma^2 P_{Z_1}} + \frac{(P(Z + Z^*) - \bar{P}(Z_1))^2}{\sigma^2 P_{Z+Z^*}} \quad (9)$$

where $\bar{P}(Z_1) = 60.0 \text{ GeV}/c$ is the mean Z_1 momentum in the $e^+e^- \rightarrow HZ_1$ process at the 250 GeV center-of-mass energy. All σ parameters are the mean widths of corresponding mass or momentum distributions on the reconstruction level. The combination with the minimal χ^2 is selected for the following analysis.

After jet matching is performed, several cuts are applied. To remove random backgrounds, the full visible energy in the event is required to lie in the range $200 < E(jjjj\ell^+\ell^-) < 260 \text{ GeV}$. After this cut, the dominant backgrounds come from the $e^+e^- \rightarrow W^+W^-\gamma^*$ and $e^+e^- \rightarrow ZZ\gamma^*$ processes, with the off-shell γ^* decaying to two leptons and the W and Z bosons decaying to two jets. The distribution of the off-shell photons falls sharply with increasing mass. The invariant mass of the two leptons rarely exceeds $10 \text{ GeV}/c^2$, while the mass of two leptons in the signal events starts from $10 \text{ GeV}/c^2$. To obtain the

best signal significance, the $M(\ell^+\ell^-) > 13 \text{ GeV}/c^2$ cut is applied to suppress these backgrounds. A small contribution comes from the four jets W^+W^- and ZZ backgrounds, where b or c -quarks decay semileptonically and the produced leptons split off the corresponding jet. To suppress these backgrounds, the minimum lepton momenta is required to be larger than $9 \text{ GeV}/c$. The maximum lepton momentum is required to be $P_{\max}(\ell) < 32 \text{ GeV}/c$. We also apply the cut $M(jj) > 70 \text{ GeV}/c^2$, which suppresses the contribution from the $H \rightarrow Z^*Z^*$ process. Figure 1 shows the M_Δ distributions for the signal and background events separately (a) and for the sum of the signal and background events (b), obtained as described above.

The signal distribution is modeled by the sum of two functions: a Breit-Wigner function convolved with a Gaussian function and an additional wide Gaussian function to account for residual Z^*Z^* events and a few events due to a wrong jet matching in the χ^2 selection. The width of the Breit-Wigner function is fixed to the value $\Gamma = 2.495 \text{ GeV}/c^2$, because the Z boson natural width transfers into the M_Δ value. The background is described by a third order Chebychev polynomial function. First, the signal and background distributions are fitted separately to obtain the shapes of the distributions. Then, the distribution of the sum of the signal and background contributions is fitted with the sum of the corresponding functions with fixed shapes and free normalizations. A clear signal peak is observed in the combined distribution. The fit yields 193.4 ± 24.5 signal events.

The two jet mass distributions for the Z_1 and Z bosons are shown in Fig. 2. These distributions are wide, however the large uncertainties in the jet reconstruction mostly cancel in the M_Δ distribution.

The signal significance is checked with a toy MC using the RooFit package. The 10000 M_Δ mass distributions are generated using the shapes and normalizations for the sum of the signal and background distributions obtained separately. The generated mass distributions are fitted with a function including both signal and background terms with free normalizations. Figure 3 demonstrates the distribution of the numbers of the signal events obtained from the toy MC. The fit of this distribution to the Gaussian function gives the mean value and width of 192.4 ± 0.3 and 24.9 ± 0.2 events, respectively. The toy MC results agree within uncertainties with the combined fit results. Therefore the statistical uncertainty for this channel is 12.9%. We quote as the final results the toy MC results for this and other channels.

B. Study of the $e^+e^- \rightarrow Z_1(j_1j_2)H(ZZ^*)$ process with $Z \rightarrow \ell^+\ell^-$, $Z^* \rightarrow j_3j_4$

In this channel the Z boson is reconstructed in the leptonic mode and the Z^* boson is reconstructed in the hadronic mode. The minimal χ^2 value is calculated from six possible jet combinations using the formula:

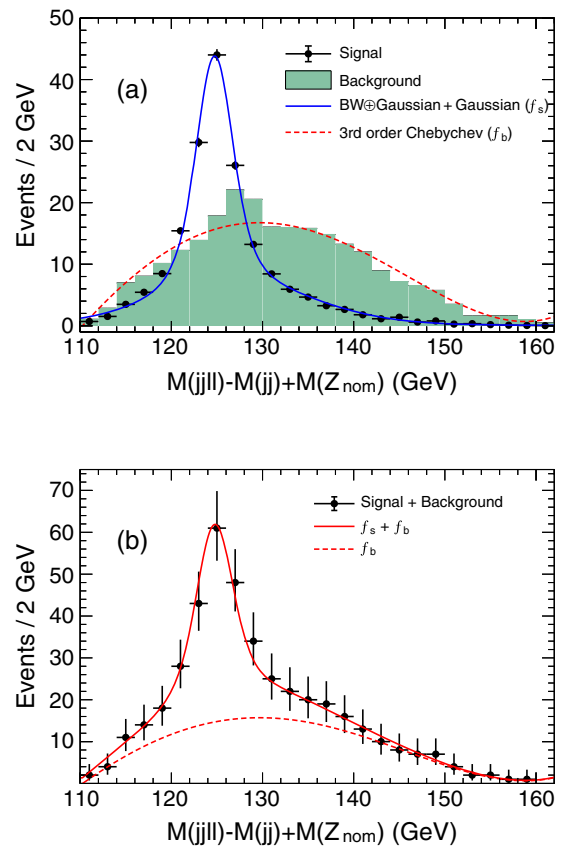


FIG. 1. The $M_\Delta = M(jj\ell\ell) - M(jj) + M(Z_{\text{nom}})$ mass distributions are shown for the $e^+e^- \rightarrow Z_1(j_1j_2)H(ZZ^*)$ process followed by the decays $Z \rightarrow j_3j_4$ and $Z^* \rightarrow \ell^+\ell^-$. (a) The distributions are presented separately for the signal (full dots) and background (shaded histogram). The fit results are overlaid: a blue solid curve for the signal and a red dashed curve for background. (b) The sum of the signal and background contributions is shown by full dots together with the fit results: red dashed curve for background and the red solid curve for the sum. The functions and the fit methods are described in the text.

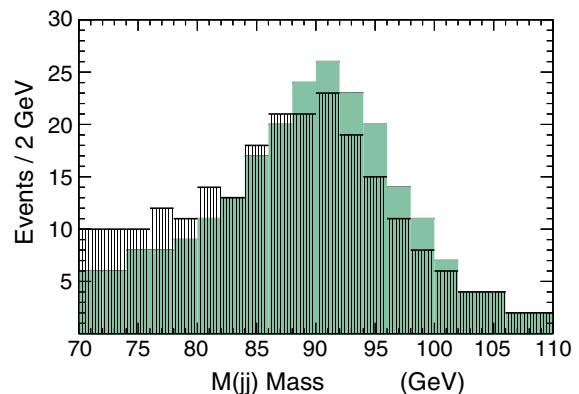


FIG. 2. The $M(j_1j_2)$ (hatched histogram) and $M(j_3j_4)$ (shaded histogram) mass distributions are shown for the $e^+e^- \rightarrow Z_1(j_1j_2)H(ZZ^*)$ process followed by the decays $Z \rightarrow j_3j_4$ and $Z^* \rightarrow \ell^+\ell^-$.

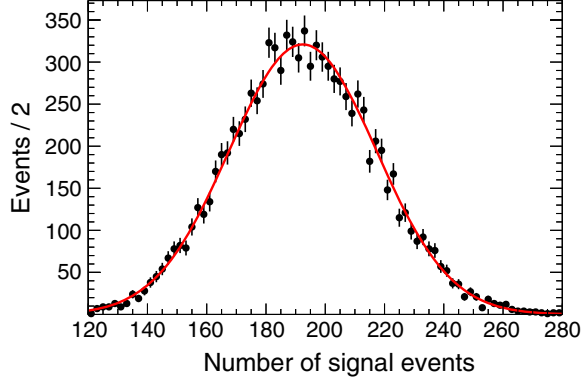


FIG. 3. The distribution of the number of the signal events obtained from the toy MC fits (dots with errors) is shown together with a fit by the Gaussian function (curve) as described in the text.

$$\chi^2 = \frac{(M(Z_1) - M(Z_{\text{nom}}))^2}{\sigma^2 M_{Z_1}} + \frac{(M(Z_1) - \bar{E}(Z_1))^2}{\sigma^2 M_{Z_1}} + \frac{(P(Z_1) - \bar{P}(Z_1))^2}{\sigma^2 P_{Z_1}} + \frac{(P(Z + Z^*) - \bar{P}(Z_1))^2}{\sigma^2 P_{Z+Z^*}} \quad (10)$$

where additionally to the $M(Z_{\text{nom}})$ and $\bar{P}(Z_1)$ values defined above, the mean Z_1 energy $\bar{E}(Z_1) = 110.0$ GeV is introduced for the $e^+e^- \rightarrow HZ_1$ process at 250 GeV. The energy term slightly improves the quality of the χ^2 selection. All σ parameters are obtained using the corresponding distributions on the reconstruction level.

We apply $70 < M(\ell\ell) < 95$ GeV/ c^2 and $200 < E(jj\ell\ell) < 260$ GeV requirements to suppress backgrounds due to random lepton pairs and possible $H \rightarrow Z^*Z^*$ contribution. Kinematically, uncorrelated lepton pairs with masses in the Z boson mass region are rarely produced at $\sqrt{s} = 250$ GeV. The cut on the di-lepton mass removes almost all combinatorial backgrounds. Additionally we reject candidates with the mass $M(jj) > 50$ GeV/ c^2 corresponding to the $Z^* \rightarrow jj$ decay. We found no significant remaining backgrounds in this channel after the application of all cuts. Figure 4 shows the distribution of the mass $M(jj\ell\ell)$, which peaks around of the Higgs boson mass. The integral of the signal distribution in the mass range $100 < M(jj\ell\ell) < 160$ GeV/ c^2 is 275.3 events. The background is very small, the integral over all bins is 18.3 events. This background is flat and can be subtracted from the final number of events. Using this method, the signal mean value and uncertainty are estimated to be 275.3 ± 17.2 events. The statistical uncertainty for this channel is 6.3%.

C. Study of the $e^+e^- \rightarrow Z_1(\nu\bar{\nu})H(ZZ^*)$ process with $Z \rightarrow jj$, $Z^* \rightarrow \ell^+\ell^-$

We also studied the processes in which the directly produced Z_1 boson decays to neutrinos. Comparing with decays in the hadronic mode, a smaller number of signal

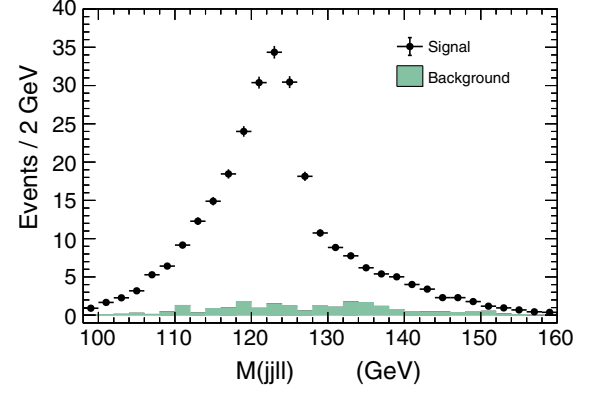


FIG. 4. The $M(jj\ell\ell)$ mass distributions are shown for the $e^+e^- \rightarrow Z_1(j_1j_2)H(ZZ^*)$ process followed by the decays $Z \rightarrow \ell^+\ell^-$ and $Z^* \rightarrow j_3j_4$. The distributions are presented separately for the signal (full dots) and background (shaded histogram).

events is expected in the neutrino mode, due to the smaller Z decay branching fraction. However the final state has a simple signature with only two jets and two leptons.

We studied different background sources to this channel with the $Z \rightarrow jj$ and $Z^* \rightarrow \ell^+\ell^-$ decays. There are many background sources with large cross sections which can contribute to this channel. Special attention must be paid to the $e^+e^- \rightarrow Z(2j)Z(\tau^+\tau^-)$ process with leptonic τ decays, and also to the $e^+e^- \rightarrow W(2j)W(\ell\nu)$ process with a lepton produced within one of the jets. Another potentially dangerous background is due to $b\bar{b}$ pair production, where both b -quarks decay semileptonically. These two leptons have to split off the jets to imitate the studied configuration. The probability for two leptons produced in hadronic jets to be identified as isolated leptons is very low, however it is compensated by high rates for this process. These backgrounds have a signature similar to the signal configuration. To reduce these backgrounds a set of cuts given in Table IV is applied. The effective cuts are on the full visible momentum $30 < P(jj\ell\ell) < 70$ GeV/ c and energy $E(jj\ell\ell) < 145$ GeV/ c . The angular cuts on the azimuthal angle of the full system relative to the beam direction, $|\cos\theta_{\text{vis}}| < 0.8$, and on the angle between the Z and Z^* boson directions, $\Delta\phi_{ZZ^*} < 120^\circ$, are used to further suppress the backgrounds. Some additional suppression of specific background configurations can be achieved if dedicated cuts are applied on the minimum and maximum momenta of the leptons. We also tested the processes $e^+e^- \rightarrow b\bar{b}$ and $e^+e^- \rightarrow ZH(b\bar{b})$ and found a small background contribution. To suppress these backgrounds we applied the $13 < M(\ell\ell) < 34$ GeV/ c^2 cut. The cut $80 < M(jj) < 113$ GeV/ c^2 is used to suppress the contribution from the $H \rightarrow Z^*Z^*$ process. Figure 5 shows the M_Δ distributions for the signal and background events separately (a) and their sum (b).

The fit procedure is applied to estimate the statistical significance. The signal is modeled with a convolution of a

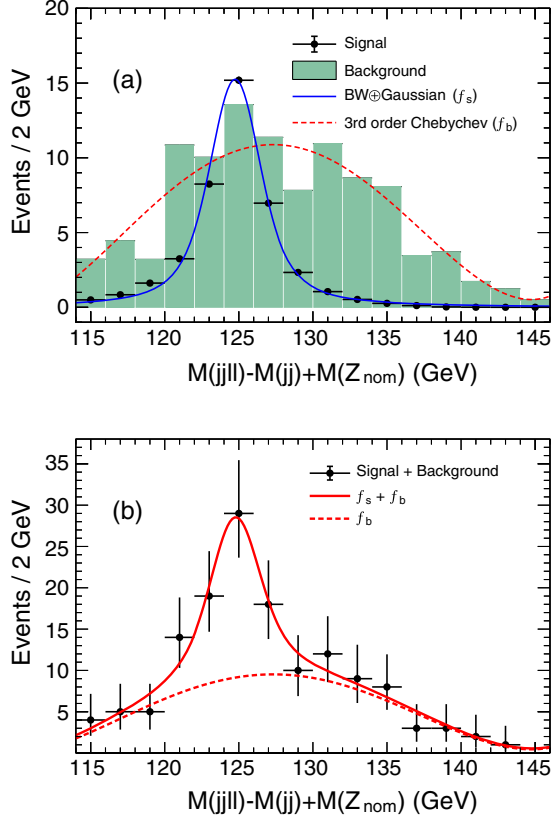


FIG. 5. The $M_\Delta = M(jj\ell\ell) - M(jj) + M(Z_{\text{nom}})$ mass distributions are shown for the $e^+e^- \rightarrow Z_1(\nu\bar{\nu})H(ZZ^*)$ process followed by the decays $Z \rightarrow jj$ and $Z^* \rightarrow \ell^+\ell^-$. (a) The distributions are presented separately for the signal (full dots) and background (shaded histogram). The fit results are overlaid: a blue solid curve for the signal and a red dashed curve for background. (b) The sum of the signal and background contributions is shown by full dots together with the fit results: red dashed curve for background and the red solid curve for the sum. The functions and the fit methods are described in the text.

Breit-Wigner function and a Gaussian function. The width of the Breit-Wigner function is fixed to the value $\Gamma = 2.495 \text{ GeV}/c^2$. The background is described by the third order Chebychev polynomial function. First, the signal and background distributions are fitted separately to obtain the shapes of the functions. Then the sum of the signal and background contributions is fitted by the sum of corresponding functions with fixed shapes and free normalizations. The fit results are shown in Fig. 5. Finally, the fit gives 52.0 ± 12.7 signal events. The toy MC estimation gives 51.9 ± 13.0 events, that results in the statistical uncertainty of 25.1%.

D. Study of the $e^+e^- \rightarrow Z_1(\nu\bar{\nu})H(ZZ^*)$ process with $Z \rightarrow \ell^+\ell^-$, $Z^* \rightarrow jj$

As in the previous channel, the Z_1 boson here decays also to neutrinos. However the hadronic and leptonic modes for the Z and Z^* bosons are swapped.

The dangerous background sources are similar to the previous channel, except the $b\bar{b}$ background. However this channel's backgrounds are more effectively suppressed due to the large dilepton mass. We select events in the intervals $80 < M(\ell\ell) < 95 \text{ GeV}/c^2$, $13 < M(jj) < 38 \text{ GeV}/c^2$, $40 < P(jj\ell\ell) < 70 \text{ GeV}/c$ and $E(jj\ell\ell) < 145 \text{ GeV}$ to suppress random lepton pairs and other backgrounds. Angular cuts $|\cos\theta_{\text{vis}}| < 0.9$ and $\Delta\phi_{ZZ^*} < 140^\circ$ are also applied. Finally we require that at least one jet from the Z^* decays has the momentum $< 22 \text{ GeV}/c$, whereas the second one has the momentum $< 42 \text{ GeV}/c$. Figure 6 shows the mass distribution $M(jj\ell\ell)$ obtained after all the cuts applied for the signal and background events separately (a) and their sum (b).

It has to be noted that the mass distribution is relatively narrow in this channel. This is because of only two jets and two leptons in the final state. Therefore we do not need to apply the minimum χ^2 method and the invariant mass of the

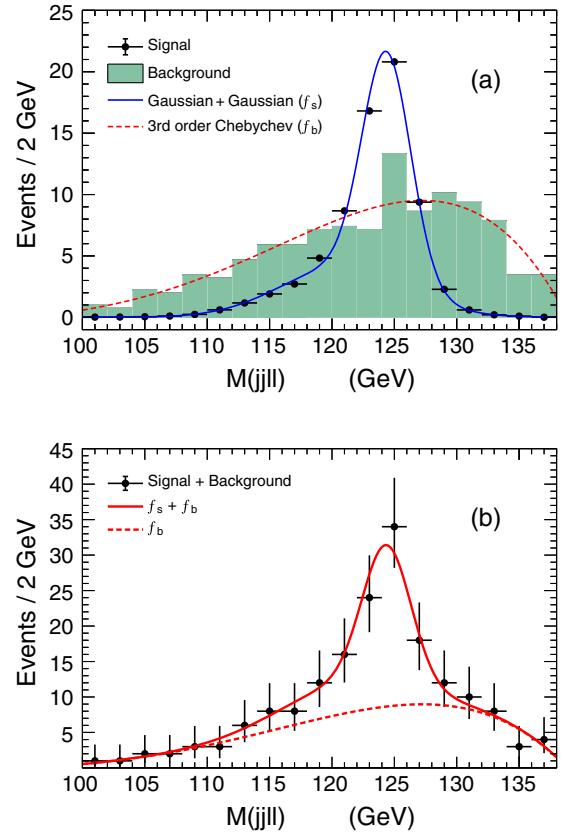


FIG. 6. The $M(jj\ell\ell)$ mass distribution is shown for the $e^+e^- \rightarrow Z_1(\nu\bar{\nu})H(ZZ^*)$ process followed by the decays $Z \rightarrow \ell^+\ell^-$ and $Z^* \rightarrow jj$. (a) The distributions are presented separately for the signal (full dots) and background (shaded histogram). The fit results are overlaid: a blue solid curve for the signal and a red dashed curve for background. (b) The sum of the signal and background contributions is shown by full dots together with the fit results: red dashed curve for background and the red solid curve for the sum. The functions and the fit methods are described in the text.

two jets will not change if some of particles are wrongly assigned to jets. The signal distribution is described by the sum of two Gaussians. The wide Gaussian accounts for the $H \rightarrow Z^*Z^*$ contribution. The background is described by the third order Chebychev polynomial function. Using the fit procedure we obtain 74.1 ± 13.9 events. The toy MC estimation gives 73.3 ± 14.2 events, corresponding to a statistical uncertainty of 19.3%. The combined fit results perfectly agree with the toy MC values in all four channels.

V. COMBINED SIGNAL SIGNIFICANCE ESTIMATE

An important result of this study is an estimate of accuracy which can be reached for the Higgs width measurement. To estimate the accuracy, we calculate the combined statistical uncertainty for the four studied channels using the formula $S_{\text{comb}} = 1/\sqrt{\sum_{i=1}^4 S_i^{-2}}$. Results obtained for all studied channels and the combined value of statistical uncertainty are given in Table V.

As given in Table V, the statistical uncertainty of the proposed method is 5.29% for the integrated luminosity 2 ab^{-1} and polarization $\mathcal{P}_{e^-e^+} = (-0.8, +0.3)$. Alternatively, we assumed two data samples with the polarizations $\mathcal{P}_{e^-e^+} = (-0.8, +0.3)$ and $\mathcal{P}_{e^-e^+} = (+0.8, -0.3)$ and the integrated luminosity of 0.9 ab^{-1} each. The same analysis is repeated for this data taking scheme and the total statistical uncertainty of 6.15% is obtained.

We note that the branching fraction $Br(H \rightarrow ZZ^*)$ will have a small contribution from the $H \rightarrow Z^*Z^*$ decay, which is around (5–10)% depending on the studied channels. This contribution can be accurately evaluated and corrected for. In the last two channels there is also a contribution from the W -fusion process $e^+e^- \rightarrow H(ZZ^*)\nu_e\bar{\nu}_e$. For the used cuts its fraction is about 15% of the selected signal events. As in the case of the previous correction, this fraction can be precisely evaluated and, therefore, does not result in a loss of accuracy.

The systematic uncertainties are not studied in this analysis. The largest systematic uncertainties are expected from the uncertainty in the selection efficiency and the uncertainty due to the signal and background shape modeling in the fit. The later systematic uncertainty will dominate. Unfortunately accurate estimates of the systematic uncertainties cannot be performed without real data.

VI. CONCLUSIONS

We studied the $e^+e^- \rightarrow HZ$ process with subsequent $H \rightarrow ZZ^*$ decay. The analysis is performed assuming the integrated luminosity 2 ab^{-1} collected at the e^+e^- collisions with center-of-mass energy 250 GeV and the beam polarizations $\mathcal{P}_{e^-e^+} = (-0.8, +0.3)$. Four channels are studied and the corresponding signal and background contributions are estimated using MC simulation. Summing results obtained in the four studied channels we obtain the combined statistical uncertainty 5.29%. This indicates, that the Higgs width can be measured using this method with an accuracy of about (5–6)% within the model-independent approach. We also repeated the analysis assuming two data samples with integrated luminosities 0.9 ab^{-1} and two beam polarizations $\mathcal{P}_{e^-e^+} = (\mp 0.8, \pm 0.3)$ and obtained the statistical uncertainty of 6.15%. The accuracy of this method is similar to one obtained in [6,7], where measurements of four or five processes have to be performed to determine the Higgs width. The results of both methods can be combined to further improve the accuracy.

The Higgs width can be potentially constrained in the future with an accuracy of about 2% by applying a global fit with many Higgs related parameters included in the frame of the effective field theory (EFT) approach [26]. Our measurement can be used to test the Higgs width value obtained within the SM, as well as within the EFT approach. Moreover, the results obtained in this analysis can be included in the global EFT fit, that can improve its

TABLE V. The fitted number of signal events and their relative statistical uncertainties obtained from the toy MC for each channel. The relative statistical uncertainties for the fitted number of signal events correspond directly to the relative statistical uncertainties for $\sigma(e^+e^- \rightarrow HZ) \times Br(H \rightarrow ZZ^*)$.

	$Z_1(jj), Z(jj),$ $Z^*(\ell\ell)$	$Z_1(jj), Z(\ell\ell),$ $Z^*(jj)$	$Z_1(\nu\bar{\nu}), Z(jj),$ $Z^*(\ell\ell)$	$Z_1(\nu\bar{\nu}), Z(\ell\ell),$ $Z^*(jj)$	Sum
$2 \text{ ab}^{-1} \text{ eLpR}$					
Number of events	192.4 ± 24.9	275.3 ± 17.2	57.9 ± 13.0	73.3 ± 14.2	-
Statistical uncertainty	12.9%	6.3%	25.1%	19.3%	5.29%
$0.9 \text{ ab}^{-1} \text{ eLpR} + 0.9 \text{ ab}^{-1} \text{ eRpL}$					
Number of events	135.2 ± 20.4	202.2 ± 14.7	30.9 ± 10.7	67.3 ± 14.3	-
Statistical uncertainty	15.1%	7.3%	34.6%	21.2%	6.15%

accuracy. Quantitatively it will be studied in a global fit for the upcoming Snowmass 2021 Higgs white paper with the input measurement from this paper.

ACKNOWLEDGMENTS

Authors are grateful to I. Bozovic-Jelisavcic, D. Jeans, J. Tian and A. F. Zarnecki for useful discussions. We would like to thank the LCC generator working group and the IL

software working group for providing the simulation and reconstruction tools and producing the Monte Carlo samples used in this study. This work has benefited from computing services provided by the ILC Virtual Organization, supported by the national resource providers of the EGI Federation and the Open Science GRID. The work is supported by the Ministry of Science and Higher Education of the Russian Federation, Agreement No. 14.W03.31.0026.

-
- [1] G. Aad *et al.* (ATLAS Collaboration), Observation of a new particle in the search for the Standard Model Higgs boson with the ATLAS detector at the LHC, *Phys. Lett. B* **716**, 1 (2012).
- [2] S. Chatrchyan *et al.* (CMS Collaboration), Observation of a new boson at a mass of 125 GeV with the CMS experiment at the LHC, *Phys. Lett. B* **716**, 30 (2012).
- [3] P. A. Zyla *et al.* (Particle Data Group), The review of particle physics 2020, *Prog. Theor. Exp. Phys.* **2020**, 083C01 (2020).
- [4] M. Cepeda *et al.* (HL/HE WG2 group), Higgs Physics at the HL-LHC and HE-LHC, *CERN Yellow Rep. Monogr.* **7**, 221 (2019).
- [5] D. de Florian *et al.* (LHC Higgs Cross Section Working Group), Handbook of LHC Higgs cross Sections: 4. Deciphering the nature of the Higgs sector, Report No. CERN Report 2017-002, 2016.
- [6] D. M. Asner *et al.*, ILC Higgs white paper, [arXiv:1310.0763](https://arxiv.org/abs/1310.0763).
- [7] C. Dürig, K. Fujii, J. List, and J. Tian, Model independent determination of HWW coupling and Higgs total width at ILC, [arXiv:1403.7734](https://arxiv.org/abs/1403.7734).
- [8] T. Behnke *et al.*, The international linear collider technical design report—Volume 4: Detectors, [arXiv:1306.6329](https://arxiv.org/abs/1306.6329).
- [9] P. Bambade *et al.*, The international linear collider: A global project, [arXiv:1903.01629](https://arxiv.org/abs/1903.01629).
- [10] W. Kilian, T. Ohl, and J. Reuter, WHIZARD: Simulating multi-particle processes at LHC and ILC, *Eur. Phys. J. C* **71**, 1742 (2011).
- [11] S. Alpin, J. Engels, F. Gaede, N. A. Graf, T. Johnson, and J. McCormick, LCIO: A persistency framework and event data model for HEP, *2012 IEEE Nuclear Science Symposium and Medical Imaging Conference (NSS/MIC 2012)* (2012), pp. 2075–2079.
- [12] T. Sjostrand, S. Mrenna, and P. Skands, PYTHIA 6.4 physics and manual, *J. High Energy Phys.* **05** (2006) 026.
- [13] R. Poeschl, Software Tools for ILC Detector Studies, *eConf C0705302*, PLE104 (2007).
- [14] A. Sailer, M. Frank, F. Gaede, D. Hynds, S. Lu, N. Nikiforou, M. Petric, R. Simoniello, and G. Voutsinas (CLICdp, ILD Collaborations), DD4Hep based event reconstruction, *J. Phys. Conf. Ser.* **898**, 042017 (2017).
- [15] F. Gaede, Marlin and LCCD-Software tools for the ILC, *Nucl. Instrum. Methods Phys. Res., Sect. A* **559**, 177 (2006).
- [16] MCParticle Class Reference, http://lcio.desy.de/v01-07/doc/doxygen_api/html/classEVENT_1_1MCParticle.html.
- [17] J. Marshall and M. Thomson, Pandora particle flow algorithm, in *Proceedings of CHEF2013—Calorimetry for the High Energy Frontier* (2013), pp. 305–315.
- [18] Generator meta data in ELOG (Logbook), <https://ild.ngt.ndu.ac.jp/elog/genmeta/>.
- [19] M. Cacciari, G. P. Salam, and G. Soyez, FastJet user manual, *Eur. Phys. J. C* **72**, 1896 (2012).
- [20] J. Tian and C. Dürig, isolated lepton finder, https://agenda.linearcollider.org/event/6787/contributions/33415/attachments/27509/41775/IsoLep_HLRec2016.pdf.
- [21] A. Hoecker *et al.*, TMVA: Toolkit for multivariate data analysis with ROOT, CERN Report No. 2007-007, 2007.
- [22] Si. Kawada, J. List, and M. Berggren, Prospects of measuring the branching fraction of the Higgs boson decaying into muon pairs at the international linear collider, *Eur. Phys. J. C* **80**, 1186 (2020).
- [23] M. Boronat, J. Fuster, I. Garcia, Ph. Roloff, R. Simoniello, and M. Vos, Jet reconstruction at high-energy electron-positron colliders, *Eur. Phys. J. C* **78**, 144 (2018).
- [24] P. Chen, T. L. Barklow, and M. E. Peskin, Hadron production in $\gamma\gamma$ collisions as a background for e^+e^- linear colliders, *Phys. Rev. D* **49**, 3209 (1994).
- [25] S. Catani, Y. L. Dokshitzer, M. H. Seymour, and B. R. Webber, Longitudinally invariant K_T clustering algorithms for hadron hadron collisions, *Nucl. Phys.* **B406**, 187 (1993).
- [26] T. Barklow, K. Fujii, S. Jung, R. Karl, J. List, T. Ogawa, M. E. Peskin, and J. Tian, Improved formalism for precision Higgs coupling fits, *Phys. Rev. D* **97**, 053003 (2018).